Image correlation spectroscopy of randomly distributed disks

Kathrin Spendier & James L. Thomas

Journal of Biological Physics

ISSN 0092-0606
Volume 37
Number 4

J Biol Phys (2011) 37:477-492
DOI 10.1007/s10867-011-9232-x

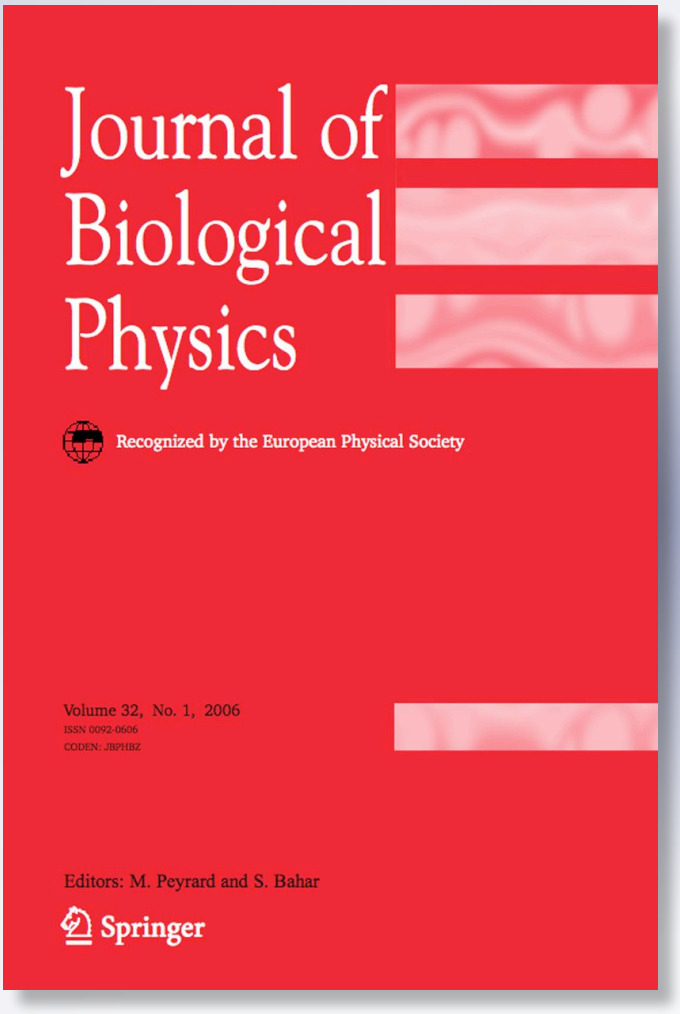

Springer

J Biol Phys (2011) 37:477–492
DOI 10.1007/s10867-011-9232-x

ORIGINAL PAPER

Image correlation spectroscopy of randomly distributed disks

Kathrin Spendier · James L. Thomas

Received: 25 May 2011 / Accepted: 18 July 2011 /
Published online: 18 August 2011

Abstract Image correlation spectroscopy (ICS) has been widely used to quantify spatiotemporal distributions of fluorescently labelled cell membrane proteins and receptors. When the membrane proteins are randomly distributed, ICS may be used to estimate protein densities, provided the proteins behave as point-like objects. At high protein area fraction, however, even randomly placed proteins cannot obey Poisson statistics, because of excluded area. The difficulty can arise if the protein effective area is quite large, or if proteins form large complexes or aggregate into clusters. In these cases, there is a need to determine the correct form of the intensity correlation function for hard disks in two dimensions, including the excluded area effects. We present an approximate but highly accurate algorithm for the computation of this correlation function. The correlation function was verified using test images of randomly distributed hard disks of uniform intensity convolved with the microscope point spread function. This algorithm can be readily modified to compute exact intensity correlation functions for any probe geometry, interaction potential, and fluorophore distribution; we show how to apply it to describe a random distribution of large proteins labeled with a single fluorophore.

Keywords ICS · Hard disk · Excluded area · Receptor clusters · Fluorescence microscopy

1 Introduction

Image correlation spectroscopy (ICS), applied to fluorescence microscopy images, has been widely used to quantify the number densities, aggregation states, and dynamics of

K. Spendier
Consortium of the Americas for Interdisciplinary Science,
University of New Mexico, Albuquerque, NM 87131, USA

K. Spendier · J. L. Thomas (✉)
Department of Physics and Astronomy,
University of New Mexico, Albuquerque, NM 87131, USA
e-mail: jthomas@unm.edu

macromolecules in cells and on cell membranes [1–8]. This technique was introduced by St-Pierre and Peterson [1] using the two-dimensional intensity autocorrelation function [2]

$$g_N(\varepsilon,\xi) = \frac{\langle i(x,y)\, i(x+\varepsilon, y+\xi)\rangle}{\langle i(x,y)\rangle^2} - 1, \tag{1}$$

where the angular brackets denote spatial averaging over all pixels in the image (x, y), and ε and ξ are spatial lag variables. With Poisson-distributed point particles, the intensity variance is proportional to the average number of particles in the diffraction-limited observation volume, after removal of the photon shot noise and the camera read noise. Since shot noise and read noise are spatially uncorrelated, they may be excluded by taking the extrapolated limit of the correlation function at zero spatial lag, rather than using the value of g_N measured there. For such an ideal system, Eq. 1 gives the average number of particles $\langle N\rangle$ in the observation volume [2]

$$\lim_{\varepsilon,\xi\to 0}\lim_{\text{Poisson}} g_N(\varepsilon,\xi) = \lim_{\text{Poisson}} \frac{\langle i(x,y)^2\rangle - \langle i(x,y)\rangle^2}{\langle i(x,y)\rangle^2} = \frac{1}{\langle N\rangle}, \tag{2}$$

where $\langle i(x,y)^2\rangle - \langle i(x,y)\rangle^2$ is the variance. Away from the origin, the shape of the correlation function is determined by the point spread function of the optics. Throughout this work, this method will be referred to as "conventional" ICS.

Real particles have a finite size, and this will modify both the shape of the correlation function (c.f.) and its extrapolated intercept at zero lag. In only moderately dense systems the particle distribution deviates significantly from Poissonian, and the relation between the estimated variance and the mean will not be as simple as given in Eq. 2. Figure 1 depicts the relation between the occupied area fraction η and the variance for a Poisson distribution and a distribution of homogenous hard disks, following Mohn and Stavem [9]. The variance for randomly distributed hard disks significantly deviates from a Poisson distribution for area fractions of 5% or more.

Thus, in dense systems conventional ICS analysis leads to a substantial overestimate of the mean number of particles in a diffraction-limited observation volume. Even though the ICS community has been aware of this effect [4, 5], thus far, high particle concentrations

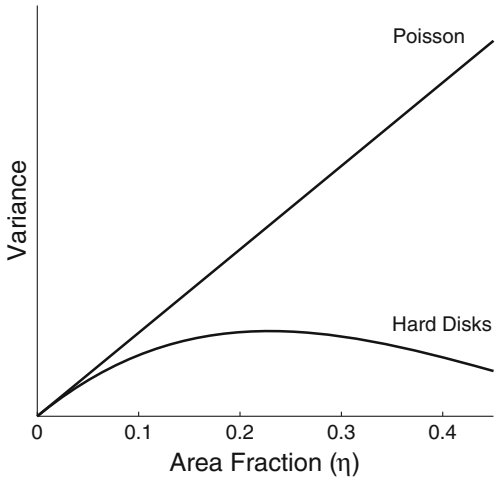

Fig. 1 Relationship between variance and occupied area fraction η for a Poisson distribution and a distribution of homogeneous hard disks, following the free area model by Mohn and Stavem [9] with a division side width of $b = 320$ arb. unit and disk radius $r = 2$ arb. unit. For high densities of disks the actual variance is less than what is predicted from the free area model [9]

have been thought to be unphysical [5] (even though interparticle interactions and area effects have been extensively studied in the context of fluorescence correlation spectroscopy [10, 11]). However, in recent investigations of the distribution of immunoglobulin E receptor microclusters on rat basophilic leukemia cells, the clusters were found to occupy an area fraction of $\eta \sim 0.30$ [8] necessitating the derivation of the intensity correlation function (c.f.) for homogeneously distributed hard disks, presented here. It is worth noting that, very recently, Kurniawan and Rajagopalan [12] extended spatiotemporal ICS to finite-sized particle systems, using a template analysis method. While template analysis gives a correct particle diffusion coefficient, it does not give mathematical relationships to compute particle number and size for finite-sized particle systems. In this work, we develop an approximate but highly accurate semianalytical algorithm to compute the correct form of the intensity c.f. for non-overlapping disks with a top-hat intensity profile. Our algorithm extends the conventional spatial ICS analysis for systems of disk-like particles, estimating particle number and size. We also show how to apply the algorithm to describe disks with a single point label (not necessarily centered). The algorithm is thus applicable for large membrane proteins with single fluorophore or quantum dot labels. Throughout this work, the new algorithm will be referred to as "hard disk" ICS.

2 Methods

2.1 Derivation of intensity correlation function

Kruglov [13] (see also the elaboration by Li et al. in [14]) has shown how the density c.f. for a system of homogeneous spheres can be derived from the pair correlation function, using geometrical considerations (the pair correlation function gives the probability of finding an object with its center at a distance r, given an object at the origin). For image correlation, the density corresponds to the image intensity. Following Kruglov, the two-dimensional density or intensity correlation for a population of disks of identical radius may be written as

$$g\left(\vec{r}\right) = \int_A g_{\text{auto}}\left(\vec{r} - \vec{r}'\right)\left[\delta\left(\vec{r}'\right) + \rho\gamma\left(\vec{r}'\right) - \rho\right] d^2\vec{r}', \tag{3}$$

where g_{auto} is the normalized density or intensity autocorrelation for a single disk, $\delta(r)$ is the two-dimensional Dirac delta function, $\gamma(r)$ is the pair c.f., and ρ is the number density of the disks. The integration is performed over the image area A. For an isotropic system, Eq. 3 may be rewritten in a symmetric form by averaging $g_{\text{auto}}(r)$ over all possible relative orientations of the vectors r and r':

$$g\left(r\right) = g_{\text{auto}}\left(r\right) + \rho\int_0^\infty\int_0^\pi g_{\text{auto}}\left(\sqrt{r^2 + r'^2 - 2rr'\cos\left(\theta\right)}\right)\left[\gamma\left(r'\right) - 1\right] 2r' d\theta dr'. \tag{4}$$

Note that g_{auto} plays a different role outside the integral (where it represents the correlation of each disk with itself) and inside the integral (where it represents the cross-correlation between disks). For uniform ('top-hat') disk fluorescence, the autocorrelation $g_{\text{auto}}(r)$ can be computed from geometry and is

$$g_{\text{auto}}\left(r\right) = \begin{cases} 1 - \dfrac{r\sqrt{R_0^2 - r^2/4}}{\pi R_0^2} - \dfrac{2}{\pi}\sin^{-1}\left(\dfrac{r}{2R_0}\right), & 0 \le r \le 2R_0 \\ 0, & 2R_0 < r \end{cases} \tag{5}$$

normalized to $g_{\text{auto}}(0) = 1$, where R_0 is the disk radius [15]. Equation 4 is the normalized per particle rotationally averaged equivalent of Eq. 1 and can be applied to systems without rotational order. The calculation of the intensity correlation function now requires the substitution of the pair c.f. into Eq. 4 and an evaluation of the integral therein.

Guo and Riebel [16] developed an analytic approximation for the pair c.f. for a monolayer of monodispersed hard disks using the Ornstein–Zernike (OZ) equation [17, 18]:

$$h\left(\vec{r}\right) = c\left(\vec{r}\right) + \rho \int_0^\infty h\left(\vec{r}'\right) c\left(\left|\vec{r} - \vec{r}'\right|\right) d\vec{r}', \tag{6}$$

where

$$h\left(r\right) = \gamma\left(r\right) + 1 \tag{7}$$

is termed the total correlation function for two particles, and $c(r)$ is termed the direct correlation function. The OZ equation reflects the "indirect" contributions of three particle correlations to the total or pair correlation function. The OZ equation is a recursive equation and can be solved using a closure relation. Guo and Riebel [16] applied the Percus–Yevick closure relation for a hard-core pair potential to approximate the direct c.f. as

$$c\left(r;\eta\right) = \Theta\left(1 - \frac{r}{2R_0}\right)\left(-\frac{1-q\eta^2}{\left(1-2\eta+q\eta^2\right)^2}\right) \times \left\{1 - a\left(\eta\right)^2\eta + \frac{2a\left(\eta\right)^2\eta}{\pi}\left[\sin^{-1}\left(\frac{r}{2R_0 a\left(\eta\right)}\right) - \frac{r}{2R_0 a\left(\eta\right)}\sqrt{1-\frac{r^2}{4R_0^2 a\left(\eta\right)^2}}\right]\right\}, \tag{8}$$

where $\Theta(r)$ is the Heaviside step function, $q = \left(4\pi\sqrt{3} - 12\right)/\pi^2$, $\eta = \rho\pi R_0^2$ is the area fraction occupied by the disks and

$$a\left(\eta\right) = 0.399\eta^4 - 1.2511\eta^3 + 2.0199\eta^2 - 0.399\eta + 2.1.$$

In Fourier space the Ornstein–Zernike equation given in Eq. 6 can be written as

$$H\left(k;\eta\right) = \frac{C\left(k;\eta\right)}{1 - \rho C\left(k;\eta\right)}, \tag{9}$$

where $H(k;\eta)$ and $C(k;\eta)$ are the Bessel transforms of the total c.f. and direct c.f., respectively, i.e.,

$$C\left(k;\eta\right) = 2\pi \int_0^\infty c\left(k;\eta\right) J_0\left(kr\right) r\, dk. \tag{10}$$

Here J_0 ( ) is the zeroth order Bessel function. Combining Eqs. 7, 8 and 9, the pair c.f. is obtained by computing the following inverse Fourier transform

$$\gamma\left(r\right) = 1 + \frac{1}{2\pi}\int_0^\infty \frac{C\left(k;\eta\right)}{1 - \rho C\left(k;\eta\right)} J_0\left(kr\right) k\, dk. \tag{11}$$

We numerically apply the Guo and Riebel direct c.f. (Eq. 8) to Eqs. 10 and 11 to find the pair c.f.; the pair c.f. is directly substituted into Eq. 4 to obtain the normalized per particle intensity correlation function.

Neglecting diffraction effects, the number of particles in a given observation volume can be determined if Eq. 4 is scaled appropriately. The scaling constant C can be obtained by computing the peak of the c.f. $g_N(0)$, where the subscript N refers to the properly normalized c.f. of N particles. Following Eq. 1, the peak of the rotationally averaged c.f., $g_N(0)$, is given as

$$g_N(0) = \frac{i^2 N\pi R_0^2 \backslash w^2}{\left[iN\pi R_0^2 \backslash w^2\right]^2} - 1 = \frac{w^2}{N\pi R_0^2} - 1 = \frac{1}{\eta} - 1, \tag{12}$$

where i describes the intensity of a homogeneous disk, w^2 is the observation area, and η is the area fraction occupied by the disks defined above. Using Eq. 12 one can compute the scaling constant C

$$C = \frac{g_N(0)}{g(0)} = \left(\frac{1}{\eta} - 1\right)\frac{1}{g(0)}, \tag{13}$$

where $g(0)$, is the peak of the normalized c.f. given in Eq. 4. Finally, the un-normalized rotationally averaged c.f. is obtained by multiplying the normalized c.f. $g(r)$, given in Eq. 4, by the scaling constant C

$$g_N(r) = \left(\frac{1}{\eta} - 1\right)\frac{g(r)}{g(0)}. \tag{14}$$

To verify Eq. 14, test images of randomly distributed hard disks with uniform intensity were created in MATLAB (The MathWorks, Natick, MA) using the DIPimage toolbox (Delft University of Technology, Delft, The Netherlands). The intensity c.f. of each test image was calculated by Fourier transform methods and rotationally averaged. Figure 2 depicts the simulated rotationally averaged c.f. $g_N(r)$ (open circles) for two test images with $R_0 = 8$ pixels, $w = 300$ pixels, $\eta = 0.05$ (Fig. 2a), and $\eta = 0.30$ (Fig. 2b). Using these parameters, the theoretical intensity c.f. obtained from Eq. 14 (solid line) was compared to the directly computed c.f. for both test images. The theoretical c.f. fits the simulated data quite well, validating the developed theory. Small deviations between simulation and theory may be attributed to the finite size and pixelation of the image, the analytic approximation of the pair correlation function, and the numerical implementation of the Bessel transforms.

2.2 Derivation of hard disk ICS

In the presence of diffraction, a fluorescence microscope image is mathematically obtained by the convolution of the point spread function (PSF) with the source distribution. In this case, the c.f. cannot be readily normalized as described above, owing to the potential overlap of the *images* of the individual disks. We have therefore chosen to leave the normalization C' of the image autocorrelation as a free (fitting) parameter; the disk size and number density are separate parameters, which will modify the autocorrelation via the direct c.f. (Eq. 8).

We approximate the PSF with a Gaussian function [19]. In polar coordinates

$$\mathrm{PSF}(r) = e^{-\frac{r}{2\sigma^2}}, \tag{15}$$

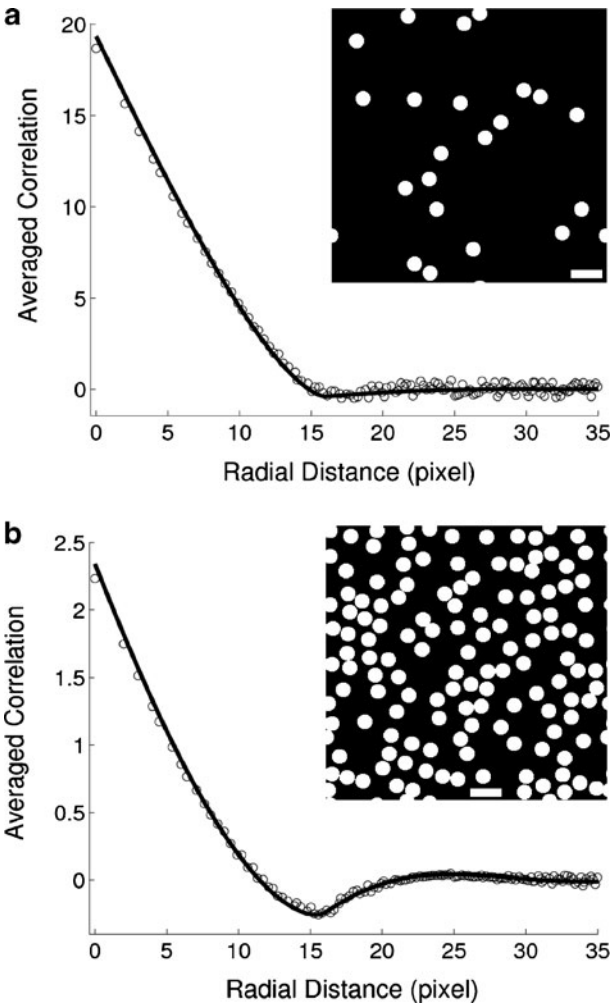

Fig. 2 Rotationally averaged spatial correlation function of two simulated distributions of hard disks with uniform intensity (*open circles*) compared to the theoretical intensity correlation function given by Eq. 14 (*solid line*) for $R_0 = 8$ pixels, $w = 300$ pixels, $\eta = 0.05$ ($N = 22$) in **a** and $\eta = 0.30$ ($N = 134$) in **b**. The theoretical intensity correlation function fits the simulated data quite well, validating the theory described in this work. *Small insets* depict the two spatially autocorrelated images. *Bar* = 32 pixels

neglecting normalization. Using the Fourier transform correlation and convolution theorems, it is straightforward to show that the autocorrelation of a convolution of two functions (real or complex) is the convolution of the autocorrelations of each function separately. Thus

$$g_{\mathrm{PSF}}(r) = C' g(r) * [\mathrm{PSF}(r) \otimes \mathrm{PSF}(r)], \tag{16}$$

where * represents convolution and $\otimes$ correlation. The autocorrelation of the Gaussian PSF given in Eq. 15 is

$$\mathrm{PSF}(r) \otimes \mathrm{PSF}(r) = e^{-\frac{r^2}{4\sigma^2}} \tag{17}$$

and the convolution in polar coordinates in Eq. 16 can be written as

$$g_{\mathrm{PSF}}(r) = C' \int_0^{\infty} \int_0^{2\pi} g\left(r''\right) e^{-\frac{\left[r^2+(r'')^2-2rr''\cos(\theta-\theta')\right]}{4\sigma^2}} d\theta' r'' dr''. \tag{18}$$

In Eq. 18, θ can be set to zero due to rotational symmetry and the integral over θ' can be evaluated, giving the hard disk ICS equation

$$g_{\mathrm{PSF}}(r) = C' \int_0^{\infty} g\left(r''\right) e^{-\frac{\left[r^2+(r'')^2\right]}{4\sigma^2}} I_0\left(\frac{rr''}{2\sigma^2}\right) r'' dr'', \tag{19}$$

where I_0 ( ) is the zeroth order modified Bessel function. C' is a scaling constant, which can be estimated by fitting Eq. 19 to the rotationally averaged intensity c.f. of the microscope image after deleting the $g_{\mathrm{PSF}}(0)$ datum (which includes uncorrelated camera shot and read noise). In general, to determine the number and radius of disk particles, the fit is made using three parameters: C', R_0, and N. The width of the Gaussian, σ, can be estimated from images of fluorescent beads that are much smaller than the microscope resolution limit, by fitting the radially averaged intensity c.f. of the bead image to Eq. 17.

2.3 Simulations of microscope images

Simulations were used to verify the developed algorithm and compare it to the conventional ICS analysis under different conditions. Test images of randomly distributed non-overlapping disks with a top-hat intensity profile were created in MATLAB using the DIPimage toolbox. Each disk, independent of its radius, and point-like particle had a constant integrated intensity of 10,000 ADU. All microscope image simulations had an image size of 640 $\times$ 640 pixels. The images were convolved with the Gaussian function given in Eq. 15 with $\sigma = 6$ pixels before adding Poisson noise. The magnitudes of the parameters were chosen to simulate an image with a pixel size of $\sim$20 nm and a typical Gaussian PSF width of $\sigma \sim 130$ nm. The intensity c.f. of each microscope test image was calculated by Fourier transform methods and rotationally averaged.

3 Results and discussion

The purpose of this work is to explore the magnitude of error caused by the application of conventional ICS analysis to finite-sized particle systems, and to present a more accurate algorithm for computing the intensity c.f. for distributions of disk-like particles. Such disk-like systems could include small receptor clusters, or protein complexes in which each subunit is fluorescently labelled (we also show how to modify the formulae to describe large proteins with a single label, below). The conventional ICS analysis assumes point-like particles and approximates the intensity c.f. by a Gaussian function reflecting the point spread function of the microscope optics. Following this ICS methodology [2] the rotationally averaged c.f. is

$$g_{\mathrm{ICS}}(r) = g_{\mathrm{ICS}}(0)\, e^{-\frac{r^2}{4\sigma_{\mathrm{ICS}}^2}}, \tag{20}$$

where $g_{ICS}(0)$ and σ_{ICS} are fitting parameters and the average number of particles N_{ICS} in the diffraction limited observation volume can be estimated by evaluating

$$N_{ICS} = \frac{\text{image area}}{g_{ICS}(0)\,\pi 4\sigma_{ICS}^2}. \tag{21}$$

In Eqs. 20 and 21 the subscript refers to parameters estimated by the conventional method. In order to compare conventional ICS analysis to the developed hard disk ICS, microscope test images were simulated for randomly distributed disks of different radii R_0 and area fractions η. To estimate the average number of particles as well as their size, resulting rotationally averaged intensity c.f.s were fit to conventional ICS given in Eq. 20 and hard disk ICS given in Eq. 19. All fits were implemented in MATLAB; the zero spatial lag $g_N(0)$ datum, which includes uncorrelated shot noise, was discarded.

Figure 3a compares the ratio of the Gaussian width obtained from conventional ICS, σ_{ICS}, to the actual width σ for different particle radii R_0 and three area fractions; $\eta = 0.01$ (open circles), $\eta = 0.10$ (filled squares), and $\eta = 0.40$ (open triangles). In conventional ICS, data that yield a Gaussian width σ_{ICS} within 30% of the true value are typically accepted as a good fit to Eq. 20 [2, 3]. This 30% criterion is represented by the shaded area in Fig. 3a. According to Fig. 3a, for area fractions of less than 1% ($\eta = 0.01$), conventional ICS successfully detects disks with a radius larger than 1.5 σ, or 200 nm when imaged with a typical high numerical aperture objective. In other words, disks of this size give intensity c.f.s that are clearly distinguishable from point particles, by the 30% criterion. However, for higher densities with area fractions larger than 40% ($\eta = 0.40$) this criterion cannot distinguish between point-like particles and disk-like particles of radius up to 3.0 σ or 400 nm. The deterioration in distinguishability is not surprising, as at these concentrations the *images* of individual particles begin to overlap significantly, owing to diffraction. In contrast, hard disk ICS can estimate any disk radius independent of area fraction. Figure 3b shows a typical radially averaged intensity c.f. of a simulated microscope image (inset in Fig. 3b) with disks of 2.67 σ in radius covering 40% of the image area (open circles). The new algorithm fits the c.f. well (black line) giving a disk radius of $R_0 = 2.74\ \sigma$, which is within 3% of the true value. For comparison, Fig. 3b also depicts the fit to conventional ICS (gray line) which gives $\sigma_{ICS} = 1.1\ \sigma$. Even though σ_{ICS} satisfies the 30% criterion, the Gaussian approximation completely misses the oscillatory decay of the rotational averaged c.f., emphasizing the need to determine the correct form of the correlation function by the algorithm presented here.

As discussed in the introduction, it is well known that conventional ICS overestimates the average number of disks for moderate area fractions. Figure 4a depicts the ratio of the number N_{FIT} obtained from conventional ICS (filled circles) and hard disk ICS (open diamonds) to the simulated number N for different area fractions η with constant disk radius $R_0 = 0.33\ \sigma$. Even at a small disk size (~40 nm) conventional ICS significantly overestimates the real number of disks for area fractions of 5% or more. For area fractions of 40% or more N_{ICS} can be larger by more than an order of magnitude. In contrast, hard disk ICS accurately estimates the average number for all area fractions as shown in Fig. 4a (open diamonds), verifying the accuracy of the developed algorithm. For disk radii significantly smaller than the laser beam radius, both conventional ICS and hard disk ICS fit the spatial correlation function very well. Figure 4b depicts typical fits to the intensity c.f. of a simulated microscope image with disks of radius $R_0 = 0.33\ \sigma$ covering an area fraction of 40%. Both conventional ICS (gray line) and hard disk ICS (black line) fit the

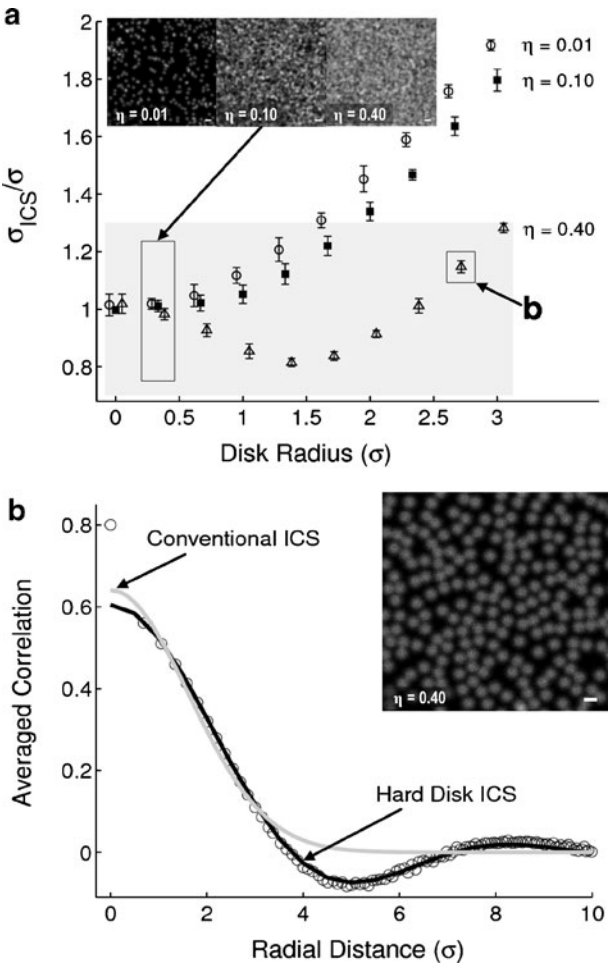

Fig. 3 In panel **a**, we show the ratio of σ_{ICS} obtained from conventional image correlation spectroscopy (ICS) analysis, Eq. 20 fitted within a 4 σ radius, to true σ for different disk radii R_0 and three area fractions η; $\eta = 0.01$ (*open circles*), $\eta = 0.10$ (*filled squares*), and $\eta = 0.40$ (*open triangles*). *Error bars* represent the standard deviation of ten simulations and the *shaded area* represents σ_{ICS} within 30% of the true value, typically representing a good fit to conventional ICS. Even though σ_{ICS} falls within the 30% criterion, conventional ICS cannot distinguish between point-like particles and disk-like particles of disk radii up to 3.0 σ. Small insets depict typical simulated microscope images for disks of 0.66 σ in diameter for $\eta = 0.01$ ($N = 326$), $\eta = 0.10$ ($N = 3259$) and $\eta = 0.40$ ($N = 13038$). Data points are offset for visualization purposes. Panel **b** shows rotationally averaged c.f. of image in *inset* for 204 disks of radius $R_0 = 2.67\ \sigma$ and $\eta = 0.40$. Hard disk ICS, Eq. 19 fitted within a 14 σ radius with fixed σ, follows the c.f. well (*black line*) estimating a disk radius of 2.74 σ. In contrast, conventional ICS (*gray line*) with σ_{ICS} satisfying the 30% criterion, completely misses the oscillatory decay of the rotational averaged correlation function. *Bar* $= 6\ \sigma$

intensity c.f. (open circles) very well. However the estimated number from conventional ICS overestimates the true value by an order of magnitude (Fig. 4a) whereas hard disk ICS gives an estimate within 20%.

The algorithm in Eq. 4 with the approximate hard disk pair c.f. $\gamma(r)$ can be applied to other isotropic systems, such as large proteins labeled with a single fluorophore at the center.

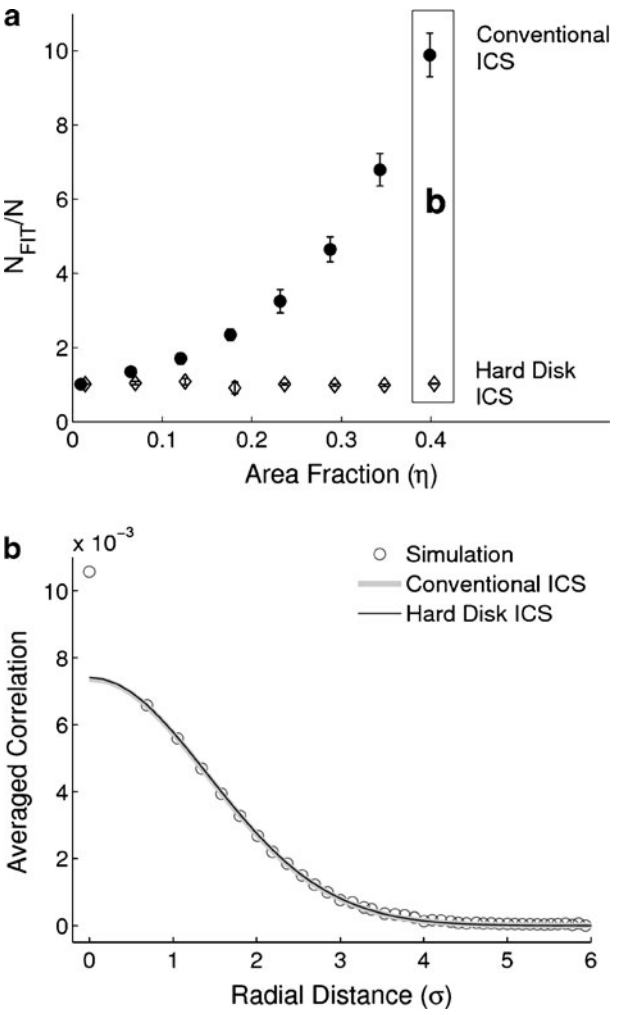

Fig. 4 In panel **a**, we show the ratio of the number N_{FIT} obtained from conventional image correlation spectroscopy (ICS) (*filled circles*, Eq. 20) and hard disk ICS (*open diamonds*, Eq. 19) to the simulated number N for different area fractions η with constant disk radius $R_0 = 0.33\,\sigma$. Conventional ICS significantly overestimates the real number of disks for area fractions of 5% or more whereas hard disk ICS gives the correct value over all area fractions within 20%. *Error bars* represent the standard deviation of ten simulations for conventional ICS and three simulations for hard disk ICS. Data points are offset for visualization purposes. For disk radii significantly smaller than the laser beam radius, both conventional ICS and hard disk ICS are expected to fit the intensity correlation function well. For example, as shown in panel **b**, for $R_0 = 0.33\,\sigma$ and $\eta = 0.40$ ($N = 13038$), conventional ICS (*gray line*) and hard disk ICS (*black line*) fit the autocorrelation function of a simulated image (*open circles*) very well. However, the estimated number from conventional ICS overestimates the true value by an order of magnitude, whereas hard disk ICS gives an estimate within 20%

For a disk with a point-like label at its center, the autocorrelation equals the normalized two-dimensional delta function $g_{\mathrm{auto}}(r) = \delta(r)/r$. Thus, the intensity c.f. convolved with the (autocorrelated) microscope PSF for a protein of radius R_0 labeled with a single fluorophore at the center is

$$g_{\mathrm{PSF}}(r) = C' \left\{ e^{-\frac{r^2}{4\sigma^2}} + \rho \int_0^\infty e^{-\frac{(r-r')^2}{4\sigma^2}} \left[\gamma\left(r'\right) - 1\right] 2r'\,dr' \right\}, \tag{22}$$

with $\gamma(r)$ computed as above, using area fraction $\eta = \rho\pi R_0^2$. Equation 22 can be used to estimate the radius as well as the number of proteins in the observation volume. Figure 5 shows a fit of Eq. 22 (solid line) to the intensity c.f. of a simulated image (open circles) of proteins 1.3 σ in diameter covering an area fraction of 30%. The new algorithm estimates

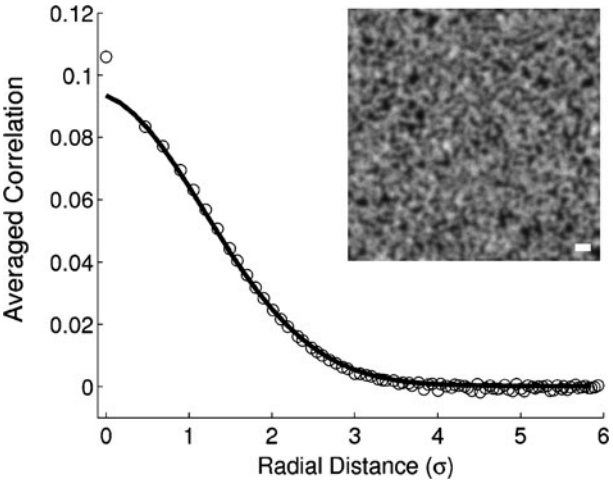

Fig. 5 Rotationally averaged intensity correlation function of a simulated microscope image (*inset* with $\sigma = 6$ pixels) of 2,200 proteins 1.3 σ in diameter, labeled with a single fluorophore at the center (*open circles*) compared to the theoretical intensity correlation function given by Eq. 22 (*solid line*) for $w = 600$ pixels and $\eta = 0.30$. Equation 22 fits the data with fixed σ quite well, estimating $R_0 = 0.65\,\sigma$ and the number of proteins ($N_{\mathrm{FIT}} = 2270$) within 5%. In contrast, conventional image correlation spectroscopy analysis, given in Eq. 20 (fit not shown), overestimates the true value by a factor of five. *Bar* $= 6\,\sigma$

the true number as well as protein size within 5%. In contrast conventional ICS (fit not shown) overestimates the true value by a factor of five.

Another geometry for which the hard disk pair correlation function can be applied is a random distribution of hard rings. Such a geometry might be appropriate to describe, for example, certain multisubunit channels or receptors in which each subunit is labeled. From geometry one can derive the normalized autocorrelation for a ring $g_{\mathrm{auto,ring}}$ of inner radius R_1 and outer radius R_2 as given in Eqs. A.1 and A.2 in the Appendix. Following the presented algorithm, the approximate theoretical intensity c.f. convolved with the microscope PSF for a distribution of hard rings with uniform fluorescence, hard ring ICS, is given in Eq. A.7. With the test image shown, fitting returned the true parameters to within 10%.

We outline a procedure suitable for large proteins, each with a single, off-center label at the same distance from the protein center. In this case, the different roles for g_{auto} in Eq. 4 must be explicitly considered. The term outside the integral is the pure autocorrelation, which is a delta function for a point label, $g_{\mathrm{auto}}(r) = \delta(r)/r$. The term inside the integral is an effective cross-correlation, which is to be averaged over all orientations. The orientationally averaged cross-correlation of two off-center labels is the same as the cross-correlation of two infinitesimally thin annular rings given in Eq. A.10 in the Appendix. We note, however, that the accuracy of the model depends on having a sufficiently large population that all relative *angular* orientations of the proteins occur with approximately equal frequency; no such requirement exists for rotationally symmetric rings or disks. Therefore, extracting parameters such as the protein diameter and label location for singly labelled proteins from ICS is likely to be experimentally demanding.

Following the steps outlined here, one can derive the analytical intensity c.f. for any probe geometry, interaction potential, and fluorophore distribution from Eq. 3. For example, for any given interaction potential $V(r)$ the Ornstein–Zernike equation, Eq. 6, is solved by

applying the following closure relation which relates $h(r)$ and $c(r)$ to the pair correlation function [18, 20]

$$\gamma\,(r) = e^{-\frac{V(r)}{k_B T}} e^{h(r)-c(r)+b(r)}, \tag{23}$$

where k_B is the Boltzmann's constant, T the temperature, and $b(r)$ the bridge function (which is typically neglected). To obtain the intensity c.f. of hard disks, $b(r)$ is set to zero and the Percus–Yevick approximation (which expands the second exponential to linear order) and a hard-core potential were applied. For a review on different closure relations and potential models the reader is referred to Li et al. [18] and references therein.

Throughout this work, we have assumed that all particles are identical and that the distribution of fluorescent sources within a particle is known. In the case of identical particles, that distribution may sometimes be determined from external knowledge: for example, a large protein may be engineered with a single, genetically encoded fluorophore at a position known from crystal structure. In the case of an annular protein complex, it may be known that every subunit is labeled (in the case of protein complexes or clusters, we note that the random absence of labels from some subunits will not affect the form of the image autocorrelation, merely its amplitude). If the label distribution is unknown, it may be possible to determine it from control experiments on dilute proteins, using deconvolution algorithms as outlined in [21, 22] and references therein.

Lastly, it is important to recognize that, although (random) variations in labeling do not affect the validity of the results, variations in the underlying structural elements would. To allow for such variation, one must use a modified pair correlation function that appropriately weights the different species.

4 Conclusions

The analytical intensity correlation function for hard disks was derived, using geometric considerations and the pair correlation function, as determined via the Ornstein–Zernike equation. Though not simply expressible, the correlation function, convolved with the microscope PSF autocorrelation, is readily implementable in computer-based fitting algorithms. It extends the conventional ICS analysis, which assumes point-like particles, to disk-like particles of uniform fluorescence intensity, which we term "hard disk ICS". The hard disk pair correlation function is readily applied to describe ICS of large proteins, with labels on center, and hard rings. We have simulated microscope images and compared the new semianalytical algorithm to the conventional method under different conditions. The results show that for large area fractions conventional ICS fails to detect disks significantly smaller than the laser beam radius. Moreover, conventional ICS significantly overestimates the average number of disks for area fractions of 5% or more, which is equivalent to a density of ten large proteins (i.e., 80 nm in diameter) per μm^2. In contrast, hard disk ICS accurately estimates the number and size of disks in an image for any area fraction and should therefore be applied to distributions of disk-like objects and high particle densities in which excluded area effects occur.

Acknowledgements K.S. was supported in part by the Program in Interdisciplinary Biological and Biomedical Sciences funded by the University of New Mexico and by Award Number T32EB009414 from the National Institute of Biomedical Imaging and Bioengineering. The content is solely the responsibility of the authors and does not necessarily represent the official views of the National Institute of Biomedical Imaging and Bioengineering or the National Institutes of Health.

Appendix: Hard ring image correlation spectroscopy

The normalized intensity autocorrelation function of a ring of inner radius R_1 and outer radius R_2 can be derived from geometrical considerations. For $2R_1 \leq (R_2 - R_1)$ the c.f. can be written as

$$g_{\text{auto,ring}}(r;\, R_1,\, R_2) = \frac{1}{\left(R_2^2 - R_1^2\right)} \begin{cases} R_2^2 - R_1^2, \; r = 0 \\ R_2^2 g_{\text{auto}}(r;\, R_2) - R_1^2 g_{\text{auto}}(r;\, R_1) - 2R_1^2 \left[1 - g_{\text{auto}}(r;\, R_1)\right], \\ \quad 0 < r < 2R_1 \\ R_2^2 g_{\text{auto}}(r;\, R_2) - 2R_1^2, \; 2R_1 \leq r \leq (R_2 - R_1) \\ R_2^2 g_{\text{auto}}(r;\, R_2) - 2R_1^2 g_{\text{cross}}(r), \; (R_2 - R_1) < r < (R_2 + R_1) \\ R_2^2 g_{\text{auto}}(r;\, R_2), \; (R_2 + R_1) \leq r < 2R_2 \\ 0, \; \text{otherwise} \end{cases} \tag{A.1}$$

and for $(R_2 - R_1) \leq 2R_2$ one obtains

$$g_{\text{auto,ring}}(r;\, R_1,\, R_2) = \frac{1}{\left(R_2^2 - R_1^2\right)} \begin{cases} R_2^2 - R_1^2, \; r = 0 \\ R_2^2 g_{\text{auto}}(r;\, R_2) - R_1^2 g_{\text{auto}}(r;\, R_1) - 2R_1^2 \left[1 - g_{\text{auto}}(r;\, R_1)\right], \\ \quad 0 < r \leq (R_2 - R_1) \\ R_2^2 g_{\text{auto}}(r;\, R_2) - R_1^2 g_{\text{auto}}(r;\, R_1) - 2R_1^2 \left[g_{\text{cross}}(r) - g_{\text{auto}}(r;\, R_1)\right], \\ \quad (R_2 - R_1) < r < 2R_1 \\ R_2^2 g_{\text{auto}}(r;\, R_2) - 2R_1^2 g_{\text{cross}}(r), \; 2R_1 \leq r < (R_2 + R_1) \\ R_2^2 g_{\text{auto}}(r;\, R_2), \; (R_2 + R_1) \leq r < 2R_2 \\ 0, \; \text{otherwise} \end{cases} \tag{A.2}$$

In Eqs. A.1 or A.2 g_{auto} is given in Eq. 5 and from geometry the normalized intensity cross-correlation function g_{cross} of two disks of radius R_1 and R_2 ($R_1 \neq R_2$) is

$$g_{\text{cross}}(r) = \begin{cases} 1, \; 0 \leq r \leq (R_2 - R_1) \\ \dfrac{\theta R_2^2}{\pi R_1^2} + \dfrac{\phi}{\pi} - z(r;\, R_1, R_2), \; (R_2 - R_1) < r < (R_2 + R_1) \\ 0, \; \text{otherwise} \end{cases} \tag{A.3}$$

with

$$z(r;\, R_1, R_2) = \begin{cases} \dfrac{hr}{\pi R_1^2}, \; \phi < 90 \\ \dfrac{R_2^2}{\pi R_1^2} \cos(\theta) \sin(\theta), \; \phi = 90 \\ \dfrac{R_2^2}{\pi R_1^2} \cos(\theta) \sin(\theta) - \dfrac{h\sqrt{R_1^2 - h^2}}{\pi R_1^2}, \; \text{otherwise} \end{cases} \tag{A.4}$$

where $h = R_2 \sin(\theta) = R_1 \sin(\phi)$, $\theta = \cos^{-1}\left(\frac{R_2^2+r^2-R_1^2}{2R_2 r}\right)$, and $\phi = \cos^{-1}\left(\frac{R_1^2+r^2-R_2^2}{2R_1 r}\right)$. Equations A.1 or A.2 can be substituted into Eq. 4 instead of the normalized intensity c.f. of a disk, Eq. 5, to obtain the rotationally averaged c.f. of randomly distributed hard rings with a uniform intensity profile, $g_{\text{ring}}(r)$, where the area fraction is defined as $\eta = \rho\pi R_2^2$ in Eq. 8. To estimate the number of rings in a given observation volume one has to compute the appropriate scaling constant. Following Eq. 1 the scaling constant is given as

$$C_{\text{ring}} = \left[\frac{w^2}{N\pi\left(R_2^2 - R_1^2\right)} - 1\right] \frac{1}{g_{\text{ring}}(0; R_1, R_2)} \tag{A.5}$$

and the un-normalized rotationally averaged intensity c.f. for hard rings can be computed by evaluating

$$g_{N,\text{ring}}(r) = \left[\frac{w^2}{N\pi\left(R_2^2 - R_1^2\right)} - 1\right] \frac{g_{\text{ring}}(r; R_1, R_2)}{g_{\text{ring}}(r; R_1, R_2)}. \tag{A.6}$$

Equation A.6 was verified by simulating a test image (inset in Fig. 6a) of rings with inner radius $R_1 = 5$ pixels and outer radius $R_2 = 10$ pixels, $w = 600$ pixels, $\eta = 0.30$. These parameters were used to compute the theoretical intensity c.f. for hard rings. Figure 6a shows that the theoretical c.f. (solid line) fits the simulated data (open circles) quite well, verifying that the presented algorithm can also be applied to distributions of hard rings as expected. Following the presented algorithm one can obtain an expression for hard ring ICS by convolving Eqs. A.1 or A.2 with the autocorrelation of the Gaussian PSF:

$$g_{\text{PSF}}(r) = C' \int_0^\infty g_{\text{ring}}\left(r''\right) e^{-\frac{\left[r^2+(r'')^2\right]}{4\sigma^2}} I_0\left(\frac{rr''}{2\sigma^2}\right) r'' dr''. \tag{A.7}$$

C' is a scaling constant which can be estimated by fitting Eq. A.7 to the rotationally averaged intensity c.f. of a microscope image after deleting the $g_{\text{PSF}}(0)$ datum. Figure 6b shows the best fit (solid line) to the intensity c.f. (open circles) of a simulated microscope image (inset). Hard ring ICS fits the intensity c.f. of the blurred image very well even though one cannot distinguish between disks or rings by eye. Hard ring ICS estimates the true number of rings within 5%. The estimate of the inner radius R_1 is 0.78 σ and of the outer radius R_2 is 1.66 σ. Both values are within 10%.

Note that the correlation function of two infinitely narrow rings can be calculated exactly and gives a simple form. The correlation function for two infinitely narrow rings, each of radius R, is obtained by writing each ring as a delta function and calculating the overlap integral. With one ring centered at the origin and the other at r, the correlation is

$$g_{\text{auto},\delta-\text{ring}}(r) = \int_0^\infty \int_0^{2\pi} \frac{1}{4\pi^2 (r')^2} \delta\left(r' - R\right) \delta\left(r' - \left[r^2 + R^2 + 2rR\cos\theta'\right]^{1/2}\right) r' dr' d\theta', \tag{A.8}$$

where the prefactors are normalizations for the delta functions, and the law of cosines was used (θ' is the angle between the point of interest in the plane and the line between ring

centers). The integral over r' is carried out by applying the first delta; to compute the integral over θ', the second delta is treated as a function of θ'. Then

$$\delta\left(f(\theta')\right) = \sum_{\theta_0'} \frac{\delta\left(\theta - \theta_0'\right)}{|f\left(\theta_0'\right)|}, \tag{A.9}$$

where the summation is taken over the zeroes of f, where $\theta' = \theta_0'$. When the rings overlap, there will be two zeroes of f, corresponding to the two points of overlap, and Eq. A.8 becomes

$$g_{\text{auto},\delta-\text{ring}}(r) = \begin{cases} \dfrac{1}{2\pi^2 R}\dfrac{1}{r\sin\theta_0'}, & 0 < r < 2R \\ 0, \text{ otherwise.} \end{cases} \tag{A.10}$$

From geometry, $\sin(\theta_0') = [1 - r^2/(4R^2)]^{1/2}$, completing the derivation.

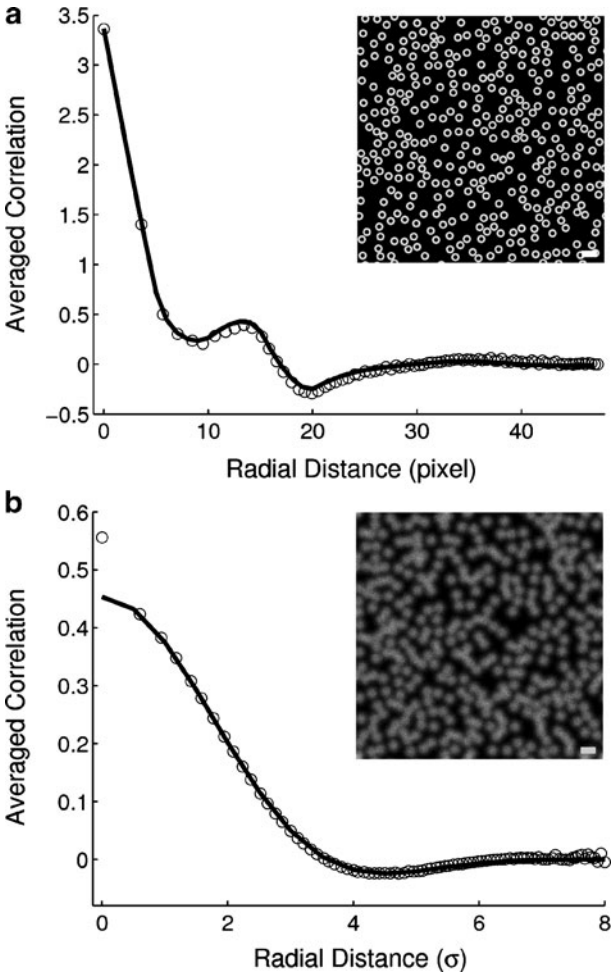

Fig. 6 Panel **a** shows the rotationally averaged spatial correlation function of a simulated distribution (*inset*) of 350 homogeneous hard rings (*open circles*) compared to the theoretical intensity correlation function given by Eq. A.6 (*solid line*) for $R_1 = 5$ pixels, $R_2 = 10$ pixels, $w = 600$ pixels, and $\eta = 0.30$. The theoretical intensity correlation function fits the simulated data quite well, validating the developed theory. *Bar* = 36 pixels. **b** Depicts the best fit (*solid line*) to the intensity correlation function (*open circles*) of a simulated microscope image (*inset*). Simulation parameters are the same as in **a** with $\sigma = 6$ pixels. Hard ring image correlation spectroscopy (ICS) given in Eq. A.7 fits the intensity c.f. of the blurred image very well even though one cannot distinguish between disks or rings by eye. Hard ring ICS estimates the true number of rings N, the inner radius R_1 as well as the outer radius R_2 within 10%, holding σ constant. *Bar* = 6 σ

References

1. St-Pierre, P.R., Petersen, N.O.: Average density and size of microclusters of epidermal growth factor receptors on A432 cells. Biochem. **31**, 2459–2463 (1992)
2. Petersen, N.O., Höddelius, P.L., Wiseman, P.W., Seger, O., Magnusson, K.E.: Quantitation of membrane receptor distributions by image correlation spectroscopy: concept and application. Biophys. J. **65**, 1135–1146 (1993)
3. Petersen, N.O., Brown, C., Kaminski, A., Rocheleau, J., Srivastava, M., Wiseman, P.W.: Analysis of membrane protein cluster densities in situ by image correlation spectroscopy. Faraday Discuss. **111**, 289–305 (1998)
4. Costantino, S., Comeau, J.W.D., Kohlin, D.L., Wiseman, P.W.: Accuracy and dynamic range of spatial image correlation and cross-correlation spectroscopy. Biophys. J. **89**, 1251–1260 (2005)
5. Kohlin, D.L., Costantino, S., Wiseman, P.W.: Sampling effects, noise, and photobleaching in temporal image correlation spectroscopy. Biophys. J. **90**, 628–639 (2006)
6. Kohlin, D.L., Wiseman, P.W.: Advances in image correlation spectroscopy: measuring number densities, aggregation states, and dynamics of fluorescently labeled macromolecules in cells. Cell Biochem. Biophys. **49**, 141–164 (2007)
7. Keating, E., Nohe, A., Petersen, N.O.: Studies of distribution, location and dynamic properties of EGFR on the cell surface measured by image correlation spectroscopy. Eur. Biophys. J. **37**, 469–481 (2008)
8. Spendier, K., Carroll-Portillo, A., Lidke, K.A., Wilson, B.S., Timlin, J.A., Thomas, J.L.: Distribution and dynamics of rat basophilic leukemia immunoglobulin E receptors (FcεRI) on planar ligand-presenting surfaces. Biophys. J. **99**, 388–397 (2010)
9. Mohn, E., Stavem, P.: On the distribution of randomly placed discs. Biometrics **30**, 137–156 (1974)
10. Abney, J.R., Scalettar, B.A., Hackenbrock, C.R.: On the measurement of particle number and mobility in nonideal solutions by fluorescence correlation spectroscopy. Biophys. J. **58**, 261–265 (1990)
11. Wu, B., Chen, Y., Müller, J.D.: Fluorescence correlation spectroscopy of finite-sized particles. Biophys. J. **94**, 2800–2808 (2008)
12. Kurniawan, N.A., Rajagopalan, R.: Probe-independent image correlation spectroscopy. Langmuir **27**, 2775–2782 (2001)
13. Kruglov, T.: Correlation function of the excluded volume. J. Appl. Cryst. **38**, 716–720 (2005)
14. Li, X., Shew, C.-Y., Liu, Y., Pynn, R., Liu, E., Herwig, K.W., Smith, G.S., Robertson, J.L., Chen, W.-R.: Prospect for characterizing interacting soft colloidal structures using spin-echo small angle neutron scattering. J. Chem. Phys. **134**, 094504 (2011)
15. Stillinger, F.H.: Pair distribution in the classical rigid disk and sphere systems. J. Comp. Phys. **7**, 367–384 (1971)
16. Guo, X., Riebel, U.: Theoretical direct correlation function for two-dimensional fluids of monodisperse hard spheres. J. Chem. Phys. **125**, 144504 (2006)
17. Adda-Bedia, M., Katzav, E., Vella, D.: Solution of the Percus–Yevick equation for hard disks. J. Chem. Phys. **128**, 184508 (2008)
18. Li, X., Shew, C.-Y., Liu, Y., Pynn, R., Liu, E., Herwig, K.W., Smith, G.S., Robertson, J.L., Chen, W.-R.: Theoretical studies on the structure of interacting colloidal suspensions by spin-echo small angle neutron scattering. J. Chem. Phys. **132**, 174509 (2010)
19. Zhang, B., Zerubia, J., Olivo-Marin, J.-C.: Gaussian approximations of fluorescence microscope point-spread function models. Appl. Opt. **46**, 1819–1829 (2007)
20. Attard, P., Bérard, D.R., Ursenbach, C.P., Patey, G.N.: Interaction free energy between planar walls in dense fluids: an Ornstein–Zernike approach with results for hard-sphere, Lennard–Jones, and dipolar systems. Phys. Rev. A **44**, 8224–8234 (1991)
21. Holmes, T.J., Liu Y.: Richardson–Lucy/maximum likelihood image restoration algorithm for fluorescence microscopy: further testing. Appl. Opt. **28**, 4930–4938 (1989)
22. Holmes, T.J.: Blind deconvolution of quantum limited incoherent imagery: maximum-likelihood approach. J. Opt. Soc. Am. A **9**, 1052–1061 (1992)